Free Surface on a Simple Fluid between Cylinders Undergoing Torsional Oscillations. IV. Oscillating Rods

B. E. D. KOLPIN,* G. S. BEAVERS, and D. D. JOSEPH,
Department of Aerospace Engineering and Mechanics, University of Minnesota, Minneapolis, Minnesota 55455

Synopsis

In earlier papers (Parts I and II) we gave the perturbation analysis for the prediction of the free surface on a simple fluid near an oscillating rod and presented the results of a preliminary experiment involving a single rod in one sample of simple fluid. In this paper we report the results of a recent more extensive experimental investigation aimed at testing the predictions of the theroy. These experiments involve the use of two different simple fluids and three rods of differing diameters. The experimental results reinforce our earlier results and substantiate the predictions of the theory with respect to the diameter dependence of the normalized height of climb at the rod surface. The rapid increase in fluid temperature near the rod caused by shear heating is illustrated, and the asymptotic form of the theory for large angular frequencies is derived.

INTRODUCTION

This paper represents a further contribution to our work on problems associated with oscillatory motions of simple fluids. In Part I[1] of this series of papers a small amplitude theory of domain perturbations was used to develop an algorithm for the computation of the unsteady motion of a simple fluid contained between concentric cylinders when the angular frequency of the inner cylinder varies sinusoidally with time. The computation leads to expressions for the free surface involving two material functions $G(s)$ and $\gamma(s_1,s_2) = \gamma(s_2,s_1)$. Some information about these functions can be obtained

* Present address: The 3M Company, St. Paul, Minnesota 55144.

Journal of Rheology, 24(6), 719–739 (1980) 0148-6055/80/0024-0719$02.10

from experiments when appropriate forms are postulated for the two material functions. Preliminary experiments to test the theory were conducted with a circular rod undergoing torsional oscillations in a large volume of a simple fluid, and the results were reported in Part II.[1] Sturges and Joseph extended the analysis of Part I to the problem of oscillating planes, and reported their work in Part III.[2] This paper returns to the problem of a circular rod undergoing torsional oscillations in a large volume of fluid and presents the results of an experimental program designed to extend the work reported in Parts I and II.

To describe the old experimental results of Part II and the new ones of this paper we must first quote the appropriate theoretical predictions derived in Part I. The full analysis of Part I has been well summarized in an earlier review article,[3] and thus we repeat here only those results which are essential to the development of this paper.

We consider a circular rod of radius a oscillating about a vertical axis with a motion $\Omega = \varepsilon \sin \omega t$, where the amplitude ε is given by $\varepsilon = \omega\Theta/2$ and Θ is the angle of twist. At second order the height of climb at the rod, $h(a,t,\varepsilon)$, is given by

$$h(a,t,\varepsilon) = \tfrac{1}{4}[2\bar{\bar{h}}(a) + e^{2i\omega t}h_1(a) + e^{-2i\omega t}\bar{h}_1(a)]\varepsilon^2 + O(\varepsilon^4), \quad (1)$$

where "$(\bar{\ })$" denotes average values over an oscillation period $2\pi/\omega$ and "$(^-)$" denotes the complex conjugate. The climb $h(a,t,\varepsilon)$ consists of the superposition of a mean climb $\bar{\bar{h}}(a)$, independent of t, and an oscillating climb which has a frequency of 2ω. All our experiments so far show that the mean climb completely dominates the total climb except for very high values of both the oscillation frequency and the angle of twist. The steady shape of the climbing bubble for a fixed angle of twist and increasing values of the oscillation frequency is illustrated in Fig. 1. Comparison of this figure with similar figures for steady rotation of a rod[4] reveals a similarity between the bubble shapes on an oscillating rod and those on a steadily rotating rod. This similarity of shape only breaks down when bubble instability begins to be evident, as in frame (f) of Fig. 1.

The mean steady climb is given approximately, at second order,

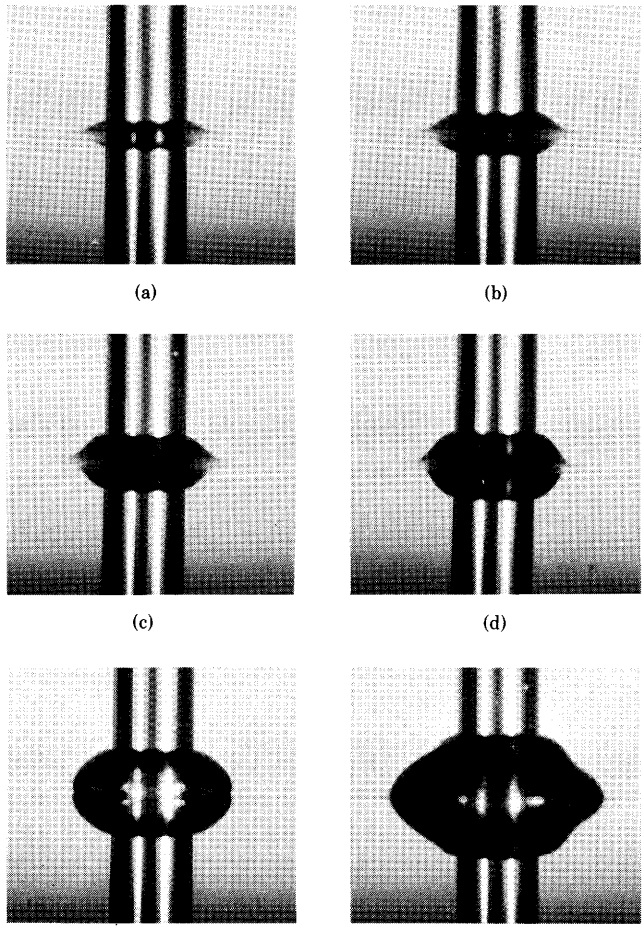

Fig. 1. Change in the free surface of TLA-227 near a rod of radius 0.636 cm as the oscillation frequency ω is increased for a constant angle of twist $\Theta = 2.97$ rad. Oscillation frequency (rad/sec): (a) 4.7; (b) 6.6; (c) 8.8; (d) 11.1; (e) 18.8; (f) 55.0.

by

$$\bar{\bar{h}}(a) = \frac{\omega^2\Theta^2}{8}\left[\frac{a}{(\rho g T)^{1/2}}\left(\frac{|\Lambda + 1|^2\hat{\beta}_\Lambda}{(\Lambda_r + 1)[2(\Lambda_r + 1) + \lambda]} - \frac{\rho a^2}{2\Lambda_r(2\Lambda_r + \lambda)}\right)\right] \quad (2)$$

where ρ is the fluid density, T is the surface tension, and $\lambda^2 = \rho g a^2/T$. The parameter $\hat{\beta}_\Lambda$ depends upon material functions which characterize the fluid, and is defined by

$$\hat{\beta}_\Lambda = -(2\Lambda_r + 1) \int_0^\infty G(s) \frac{\sin \omega s}{\omega} ds + (\Lambda_r + 1) \int_0^\infty \int_0^\infty \gamma(s_1,s_2) \cos \omega(s_1 - s_2) ds_1 \, ds_2, \quad (3)$$

where $G(s)$ is the shear relaxation modulus and $\gamma(s_1,s_2)$ is a second material function. The function Λ_r appearing in Eqs. (2) and (3) is the real part of a complex function Λ defined by

$$\Lambda^2 = 1 + a^2 A^2, \quad (4)$$

where

$$A^2 = i\rho\omega \Big/ \int_0^\infty G(s) e^{-i\omega s} ds. \quad (5)$$

Thus if the material functions $G(s)$ and $\gamma(s_1,s_2)$ are known, the height of climb at the rod can be computed at second order from Eq. (2). In particular, Eq. (2) shows that, for small amplitude motions, the normalized mean climb at the rod, given by

$$H(a,\omega) = \bar{\bar{h}}(a,\varepsilon)/\Theta^2, \quad (6)$$

is independent of the angle of twist Θ and is a universal function of the frequency ω. In general, however, the functions $G(s)$ and $\gamma(s_1,s_2)$ will not be known, and we would like to determine information about these functions from experimental measurements of the universal height rise curve. To accomplish measurements of this type we must first postulate particular forms for $G(s)$ and $\gamma(s_1,s_2) = \gamma(s_2,s_1)$. In Parts I and II we did this by defining a sequence of approximating functions $G_N(s)$ and $\gamma_M(s_1,s_2)$ which were taken as generalized Maxwell models depending on a finite number of constants to be determined from the experimentally measured height rise curve. We use the same generalized Maxwell models in this paper:

$$G_N(s) = \frac{-\mu^2}{\alpha_1} \sum_1^N \frac{a_n^2}{b_n} \exp\left(\frac{\mu}{\alpha_1} \frac{a_n}{b_n} s\right) \quad (7)$$

and

$$\gamma_M(s_1,s_2) = \alpha_2 \sum_1^M c_n k_n^2 \exp\left[-k_n(s_1 + s_2)\right], \quad (8)$$

where

$$\sum_{1}^{N} a_n = \sum_{1}^{N} b_n = \sum_{1}^{M} c_n = 1. \tag{9}$$

There are $2N + 2M - 3$ unknown constants to be determined if the constants μ, α_1, and α_2 of the fluid of second grade are known. The unknown constants associated with the first three approximations are

$N = 1, M = 1 \quad k_1;$

$N = 1, M = 2 \quad k_1, k_2, c_1;$

$N = 1, M = 3 \quad k_1, k_2, k_3, c_1, c_2.$

Our original experiments of Part II were performed with a single rod in a single sample of TLA-227, which is a concentrate of a methacrylic copolymer in oil. The results of those experiments are reproduced in the upper part of Fig. 2, where it can be seen that the experimental points for each angle of twist do indeed define part of a universal curve until they break away at some value of the oscillation frequency ω. We concluded that the points which break away from the universal curve are manifestations of effects which are induced by terms of order higher than second. Thus as an aid in the selection of the experimental points which define the universal curve we derived in Part II a very conservative estimate for the region of validity of the second-order theory:

$$\omega^2 < \frac{8g}{\Theta^2}\left[\frac{1}{a(3\alpha_1 + 2\alpha_2)}\left(\frac{\rho T}{g}\right)^{1/2}\right]^{1/2}. \tag{10}$$

For each angle of twist, the critical angular velocity [given by the right side of Eq. (10)] is indicated by a vertical bar in Fig. 2.

In attempting to fit the (N,M) models to our initial experimental results we limited ourselves to fitting the first two models of the sequence. We found that by choosing $k_1^2 = 15.43$ we were able to fit the $(N = 1, M = 1)$ model for ω^2 values up to 30 (rad/sec)^2, and by choosing $k_1^2 = 14.50$, $k_2^2 = 307$, and $c_1 = 0.9735$ we were able to fit the $(N = 1, M = 2)$ model for ω^2 values up to 450 (rad/sec)^2. These results are shown in the lower part of Fig. 2.

In this paper we report results from a much more extensive experimental investigation in which we have attempted to establish the universal normalized height rise curves for several rods of different

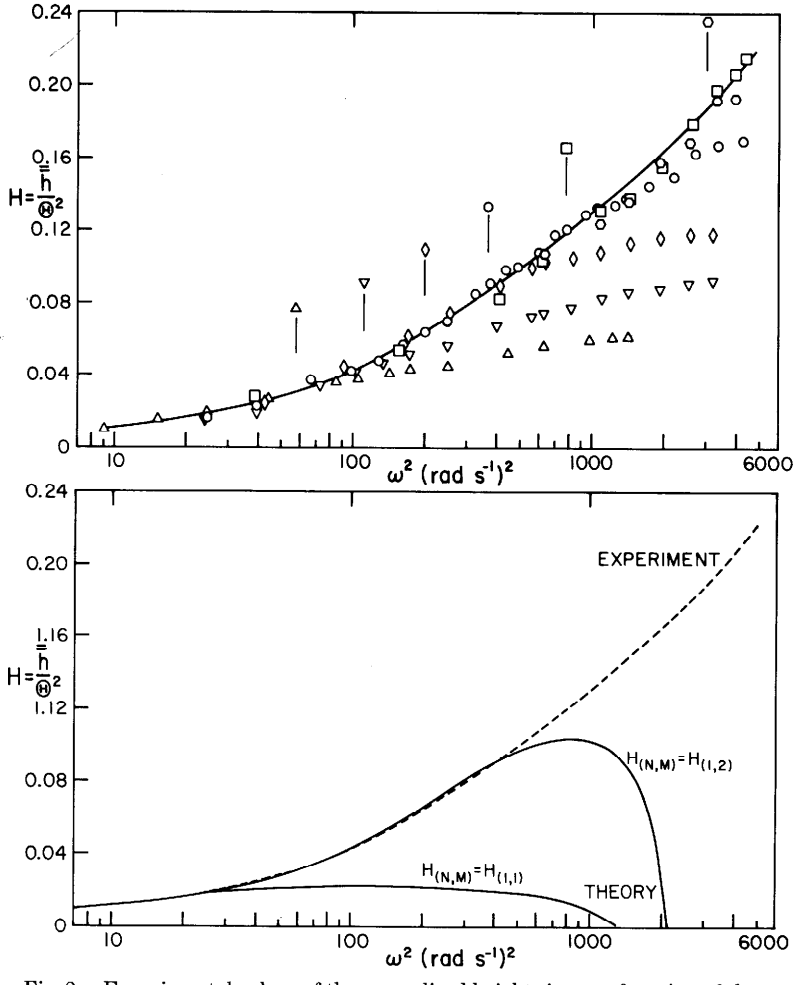

Fig. 2. Experimental values of the normalized height rise as a function of the oscillation frequency, and comparison of the experimentally determined curve with the predictions of the first two Maxwell models. Data are for a rod of radius 0.636 cm oscillating in TLA-227 at six different angles of twist. Vertical bars are values of ω_r^2 associated with the criterion given in Eq. (10). Results are taken from Ref. 1. Θ (rad): (○) 0.56; (□) 1.10; (○) 1.61; (◇) 2.18; (▽) 2.91; (△) 4.05.

diameter oscillating in two different fluids, and we have extended the model-fitting procedure to include the ($N = 1, M = 3$) model. (A full discussion of this is given in the section on "Normalized Height Rise Results" below). We also derive the asymptotic result for the mean climb at the rod for large values of the oscillation frequency ($\omega \to \infty$, $\Theta \to 0$, $\omega\Theta = \varepsilon$ is small), but we were not able to obtain corresponding experimental results due to the limitations of our apparatus.

EXPERIMENTS

Apparatus

The apparatus used for these experiments was a refined version of that employed for our original experiments.[1] The principal component of the apparatus was a circular rod which could oscillate about its axis in a large vat of liquid. The angle of twist of the motion and the oscillation frequency could be set at predetermined values. An important feature of the new apparatus was the facility to monitor the temperature of the fluid in the immediate vicinity of the rod throughout a complete experimental test.

An overall view of the apparatus is shown in the upper part of Fig. 3. The fluid was contained in a circular Plexiglas cylinder having a diameter of 30.4 cm and a depth of 7.7 cm. The drive shaft for the rod entered the container through a housing which contained bearings and seals and which was fastened to the underside of the container. Motion was imparted to the drive shaft through a rack-and-pinion mechanism, which in turn was driven from an electric motor by means of a crank consisting of an adjustable slider. The angle of twist Θ of the rod was determined by the position of the slider, which was initially calibrated by observing the motion of a radial line on the upper end of a rod through a traveling microscope fitted with a protractor eyepiece.

The oscillation frequency ω was measured by means of a system consisting of ten reflecting surfaces equally spaced around the motor drive shaft, a light source and photomultiplier tube, and a digital counter. This system was capable of measuring the frequency to within ± 0.01 rps.

Three polished aluminum rods of radii 0.320, 0.468, and 0.636 cm were used. Each rod had a screw thread at its lower end, which allowed a secure attachment and accurate alignment with the drive

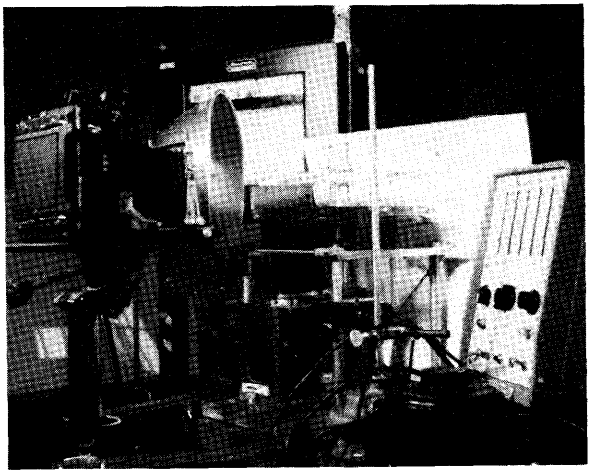

(a)

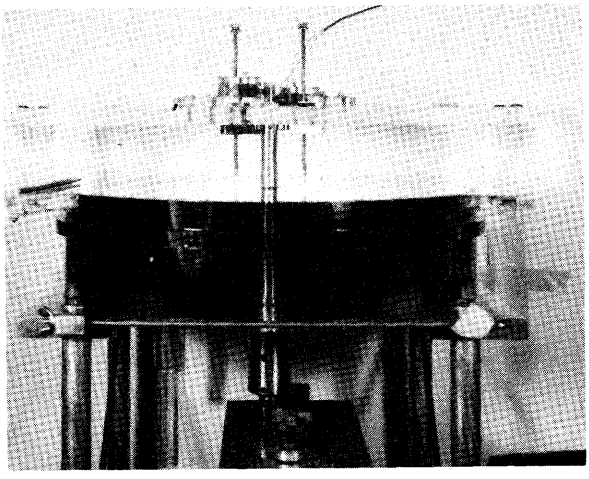

(b)

Fig. 3. Experimental equipment, showing (a) overall view and (b) details of the rod-restraining mechanism and the slip rings and brushes for the temperature measuring system.

shaft. The rod was constrained in the vertical position by means of three roller bearings located near the upper end. A flush-mounted copper–Constantan thermocouple was installed in the surface of each rod at a position approximately 1.2 cm below the free surface level of the fluid. The thermocouple wires were installed through the hollow center of each rod and wound in two separate bands around a nylon sleeve on the upper end of the rod. These bands served as slip rings for two spring-loaded brushes. A copper brush was used for the copper wire and a Constantan brush for the Constantan wire. The roller bearing containment system and the slip rings and brushes are shown in the lower part of Fig. 3.

The dimensions of the climbing bubble of liquid were determined photographically from Polaroid negatives taken at grazing incidence along the surface of the undisturbed liquid. In order to measure the bubble height from the projected negatives it was necessary to locate accurately the position of the free surface of the undisturbed liquid. This was accomplished by means of the two metal pointers shown on each side of the rod in Fig. 3. The pointers were positioned in a diametral plane normal to the direction from the camera to the rod. The vertical position of the pointers was carefully adjusted, so that the tips were as close to the surface of the liquid as possible, without actually touching it. In this way the pointers and their reflections in the liquid surface enabled the free surface in the plane of the pointers to be located.

Each rod was coated with Scotchgard, a commercial water-proofing agent, before it was inserted into the apparatus. This coating produced a horizontal contact of the fluid at the rod surface, thus eliminating the static rise due to capillarity. During the course of an experiment, data were always taken for increasing values of the oscillation frequency. This avoided prior wetting of the rod and thus satisfied the requirement that the liquid always advanced on to a dry part of the rod.

The two fluids used in these experiments were TLA-227, manufactured by the Texaco Oil Company, and Paratone 715, manufactured by the Exxon Chemical Company. Paratone 715 is an olefin polymer in oil and TLA-227 is a methacrylate copolymer in oil. Both are used commercially as viscosity index improvers. The fluid properties and characterizing coefficients through second order are given in Table I.

The values of the viscosity μ and the Rivlin–Ericksen coefficient

TABLE I
Fluid Properties of TLA-227 and Paratone 715

	TLA-227	Paratone 715
Density, ρ (g/cm^3)	0.896	0.857
Surface tension, T (dyn/cm)	30.5	30.6
Viscosity, μ (P)	200	305
α_1 (g/cm)	−50	−50
α_2 (g/cm)	83.9	82.5
$\hat{\beta}$ (g/cm)	18.0	15.05

α_1 were obtained from measurements made on a Rheometrics Mechanical Spectrometer using cone and plate flow and extrapolation to zero shear rate. The value of $\hat{\beta} = 3\alpha_1 + 2\alpha_2$ was determined from experiments with a rotating rod viscometer.[1,4] The data from which the values of $\hat{\beta}$ were computed are presented in Fig. 4 and are included here to demonstrate that both TLA-227 and Paratone 715 have measurable ranges of steady rotational speed for which the motion is well described by second-order theory. The Rivlin–Ericksen coefficient α_2 was obtained from the values of μ and α_1. We believe that the values of $\hat{\beta}$ and μ were accurately determined, but that the values for α_1 are subject to some uncertainty because of the inherent limitation of the cone and plate apparatus at low rates of shear, and

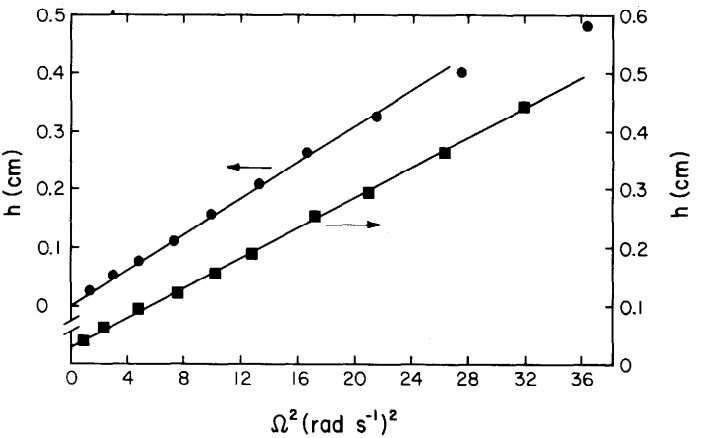

Fig. 4. Height of climb at the rod for a rod of radius 0.468 cm rotating at constant angular velocity Ω in (●) TLA-227 and (■) Paratone 715. There is a distinct range of angular velocities for which the fluids behave like second-order fluids. Slopes of the lines are used in the determination of the climbing constant $\hat{\beta}$.

also because the first normal stress difference of these fluids changes very rapidly near zero shear rate.

Preliminary Investigation of Shear Heating Effects

Temperature increases caused by shear heating of the fluid were of primary concern to us throughout these experiments. In our earlier work on the rotating rod viscometer[4] we investigated the temperature dependence of the climbing constant $\hat{\beta}$ for a solution of polyisobutylene in a petroleum oil. We found that the value of $\hat{\beta}$ for that fluid changed by a factor of 10 over a temperature range 25–50°C. We believe that a similar strong dependence of the Rivlin–Ericksen parameters on temperature exists for both TLA-227 and Paratone 715, thus requiring that we perform the present experiments under isothermal conditions. In order to determine the severity of the temperature increase of the fluid due to shear heating we carried out a preliminary experiment in which we oscillated a rod of radius 0.468 cm under the most extreme conditions that our apparatus was capable of producing. During this experiment we used thermocouples to monitor the air temperature and the fluid temperature at the surface of the rod, at a point 2.5 cm from the rod, and at a point 2.5 cm from the outside of the container. It was observed that the temperature of the fluid near the rod rose very rapidly, and that the temperature 2.5 cm from the rod lagged that close to the rod by about 2°F, whereas we were not able to detect any change in temperature near the outer perimeter of the fluid container. We then oscillated the rod in TLA-227 through an angle of twist of 3.98 rad at several oscillation frequencies and recorded the temperature of the fluid next to the rod as a function of time. Typical temperature changes with time are illustrated in Fig. 5. The fluid temperature near the rod increases rapidly during the first few minutes of shearing, but the heating effect does not quickly dissipate into the bulk of the fluid. Based on these findings we developed an experimental procedure by which we collected data rapidly so that shearing only took place over short time intervals. We were able to keep the temperature change of the fluid at the rod surface to less than 1°F through the course of every complete experimental run. The temperature of the fluid for all experiments was 80°F.

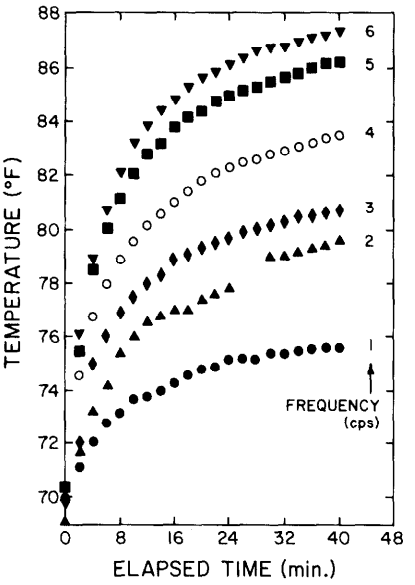

Fig. 5. Temperature of the fluid at the rod surface as a function of time when a rod of radius 0.468 cm is oscillated through an angle of twist of 3.98 rad in TLA-227 at various frequencies.

Normalized Height Rise Results

Three rods were used for the experiments with TLA-227 and two rods for the experiments with Paratone 715. The experimental data are summarized in Figs. 6 and 7, respectively, where for clarity we have shown only data which satisfy our earlier criterion [Eq. (10)] for the region of validity of the second-order theory in defining the universal curve. The theoretical height rise predictions for the generalized (N,M) Maxwell models where $(N,M) = (1,1)$, $(1,2)$, and $(1,3)$ are superimposed on the experimental results. The values of the characterizing constants of the Maxwell models were determined by requiring that the theoretical and experimental curves match over the largest possible interval $[0,\omega)$ of oscillation frequencies for all rods. The curve fitting process gave the values for the unknown fluid parameters shown in Table II.

It is interesting to note that the values obtained for k_1^2, k_2^2, and c_1 for this batch of TLA-227 are very close to those obtained in our initial experiments[1] with a prior batch of this product. We also note that,

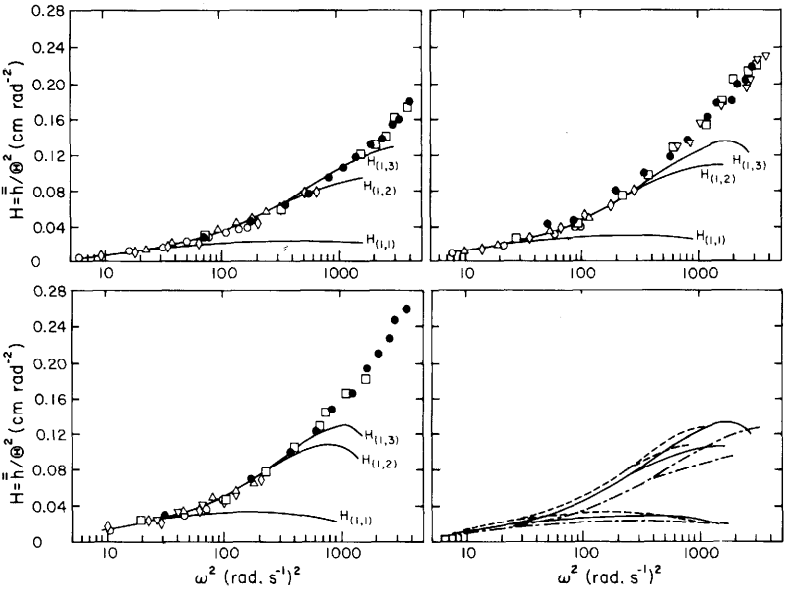

Fig. 6. Normalized height rise as a function of the square of the frequency of oscillation for three rods in TLA-227. Only experimental points that define the universal curves are shown. Predictions from the first three members of the sequence of generalized Maxwell models are compared with the experimental results. Predictions are brought together in the fourth part to show the dependence upon rod radius. Θ (rad): (▽) 0.50; (●) 0.99; (□) 1.47; (◇) 2.07; (△) 2.97; (▼) 3.50; (○) 3.98. (a) a = 0.320 cm; (b) a = 0.468 cm; (c) a = 0.636 cm; (d) a (cm): (---) 0.320; (——) 0.468; (- - -) 0.636.

with the exception of k_1^2, the values of the coefficients are very close for the two fluids tested in these experiments. This may not be totally unexpected when we observe from Table I that the Rivlin–Ericksen coefficients α_1 and α_2 are essentially the same for the two fluids, indicating that at second order we might expect very similar normal stress effects.

In the last part of Figs. 6 and 7 we have brought together the theoretical predictions for the different rod radii to show the rather weak dependence on rod radius. An increase in the rod radius produces an increase in the normalized height of climb at a fixed value of the oscillation frequency.

The results we have presented in this paper are the outcome of a much more extensive and more carefully controlled experimental

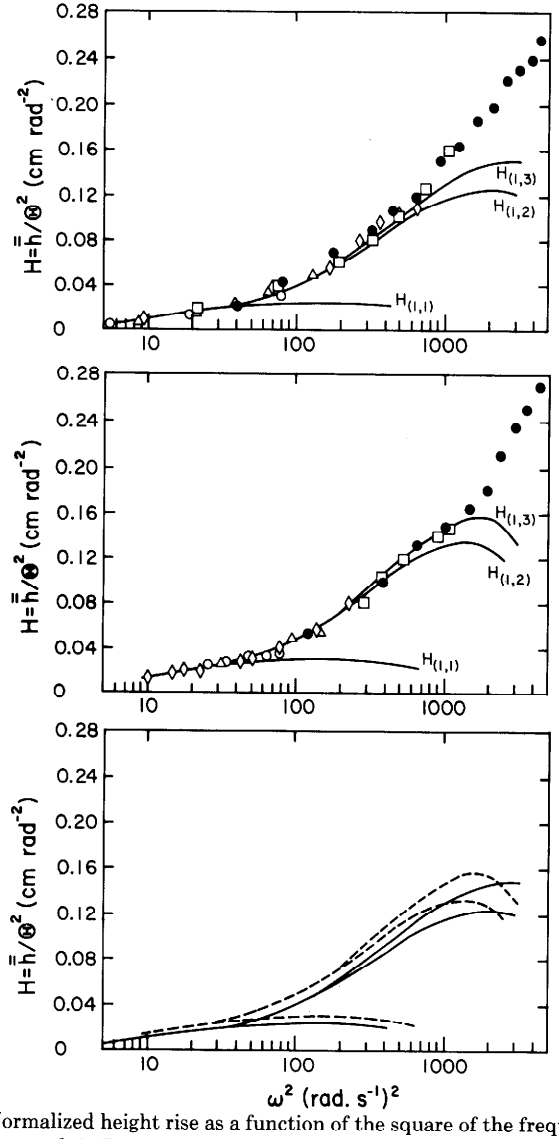

Fig. 7. Normalized height rise as a function of the square of the frequency of oscillation for two rods in Paratone 715. Only experimental points that define the universal curves are shown. Predictions from the first three members of the sequence of generalized Maxwell models are compared with the experimental results. Influence of rod radius is illustrated in the bottom part of the figure. Θ (rad): (●) 0.99; (□) 1.47; (◇) 1.93; (△) 2.97; (○) 3.98. (a) a = 0.468 cm; (b) a = 0.636 cm; (c) a (cm): (——) 0.468, (- - -) 0.636.

TABLE II
Parameter Values for the First Three Maxwell Models

	TLA-227			Paratone 715		
(N,M)	(1,1)	(1,2)	(1,3)	(1,1)	(1,2)	(1,3)
k_1^2	16.0	15.2	15.2	35.1	33.69	33.69
k_2^2		310.0	310.0		310.0	310.0
k_3^2			2000			2000
c_1		0.976	0.978		0.968	0.968
c_2			0.0184			0.0295

program than our original work.[1] The present results do not contradict our earlier findings. We are able to describe the experimental results in Part II and here with

> ... an increasing sequence of generalized (N,M) Maxwell fluids. Each fluid represents an approximation to a class of real simple fluids in small amplitude periodic motions over an increasing, but restricted, interval $I_{N,M}(\omega)$ of frequencies. The constants which are required to specify completely each fluid in the sequence may be determined by comparison with a universal function similar to that shown in Figs. 6 and 7. If the concept is good, it will be possible to predict other periodic motions of the now completely determined (N,M) fluids over similar ranges of frequency.

In reservation, we note that the Maxwell models used to describe the functions $G(s)$ and $\gamma(s_1,s_2) = \gamma(s_2,s_1)$ are just one possible representation of the material functions. The approximation of $G(s)$ with decaying exponentials has the authority of common use. But the only thing we know for sure about $\gamma(s_1,s_2)$ is that it is symmetric, $\gamma(s_1,s_2) = \gamma(s_2,s_1)$. Functions with arguments $s_1 + s_2$ have the required symmetry, but so do functions with $s_1 s_2$. So the use of decaying exponentials of argument $s_1 + s_2$ to represent $\gamma(s_1,s_2)$ is highly arbitrary.

Although it is possible to find values for the unknown coefficients which will fit the theory to the experimentally measured universal curve, the choosing of the coefficients in the Maxwell models becomes very laborious at the higher (N,M) models. We also remark that for both TLA-227 and Paratone 715 we have not been able to find any

values for a_n and b_n in Eq. (7) which improve the fit over that obtained using $a_n = 1$, $b_n = 1$, which is the $N = 1$ case.

The Flower Instability

We conclude this report on our experiments with a brief comment about an instability of the axisymmetric motion as the oscillation frequency is increased. The steady axisymmetric pattern which is evident at low values of ω loses stability to another solution with a different symmetry pattern at larger values of ω. The new symmetry pattern has a certain integral number of lobes, formed like the petals of a flower. Mathematically we characterize the flower instability as a symmetry breaking T-periodic bifurcation of a T-periodic flow. The first photographs of this phenomenon were included in Ref. 5. Since then, we have observed the instability by means of a motion picture, from which we have constructed Figs. 8 and 9. Figure 8 shows the growth of the instability for a rod oscillating at 7 cps in TLA-227. The individual frames show the rod at approximately the same position in its cycle, and the time between successive frames is approximately 1.1 sec. The final fully developed three-lobe pattern develops quite slowly, in this case taking over 50 cycles of the rod motion to grow to its final form. Once it has reached its fully developed state the petal configuration oscillates with a frequency equal to that of the rod, but with a phase lag which is determined at each radius by an outgoing wave which is supported by fluid elasticity. The phase lag is evident in Fig. 9 which shows the motion of the fully developed three-lobe pattern as the rod goes through one complete cycle of its motion.

Finally we remark that we have not yet investigated the mechanics of the instability and the parameters which lead to the number of petals which are formed. As we noted in Ref. 5, with TLA-227 we have been able to produce both three- and four-lobe patterns from what appear to be identical operating conditions. Paratone 715, which has approximately the same surface tension and steady climbing constant as TLA-227 but a somewhat higher shear viscosity, always develops a larger number of petals, usually between about 8 and 12. They are usually not as well defined as in TLA-227. Furthermore, the instability pattern in Paratone 715 rapidly entrains air bubbles, which eventually distort the pattern, whereas the flower pattern in TLA-227 will apparently persist almost indefinitely.

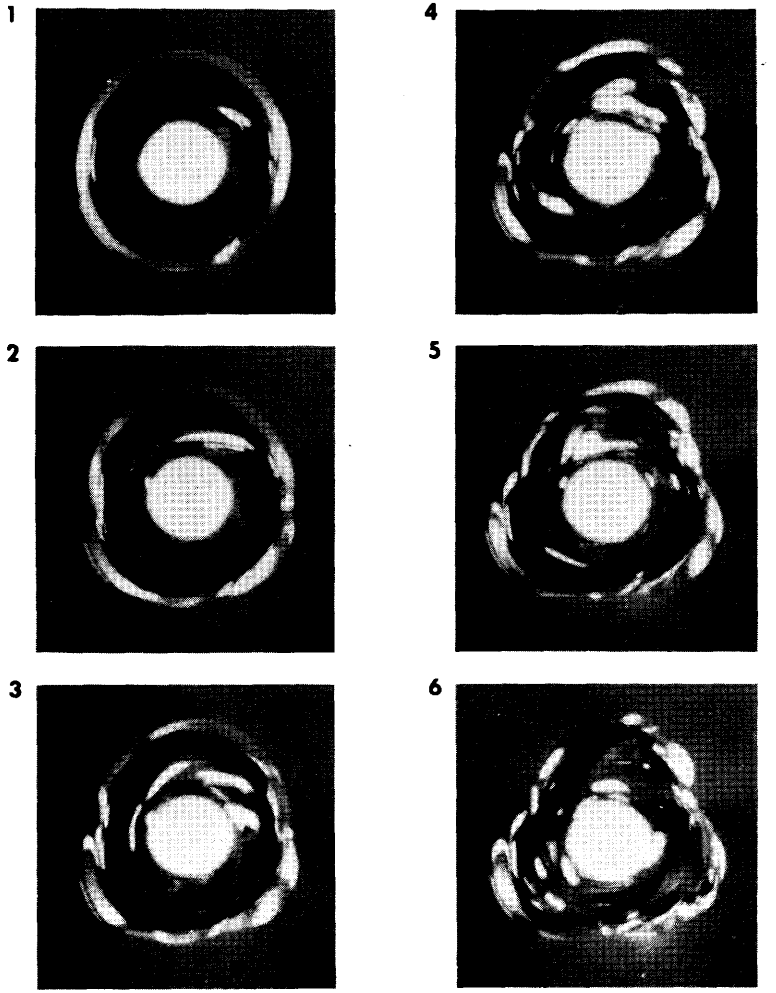

Fig. 8. Growth of the flower instability in TLA-227 as viewed from above. Rod radius is 0.636 cm, the angle of twist is 4 rad, and the frequency of oscillation is 7 cps. Rod is at approximately the same position in its cycle in each frame. Time between frames is approximately 1.1 sec. (Pictures taken from Ref. 6.)

ASYMPTOTIC HEIGHT RISE FOR LARGE ω

In our earlier work[1] we examined the asymptotic form of the height-rise prediction for the limit when the oscillation frequency becomes small. We showed that for a fixed value of $\varepsilon^2 = \omega^2\Theta^2/4$ the

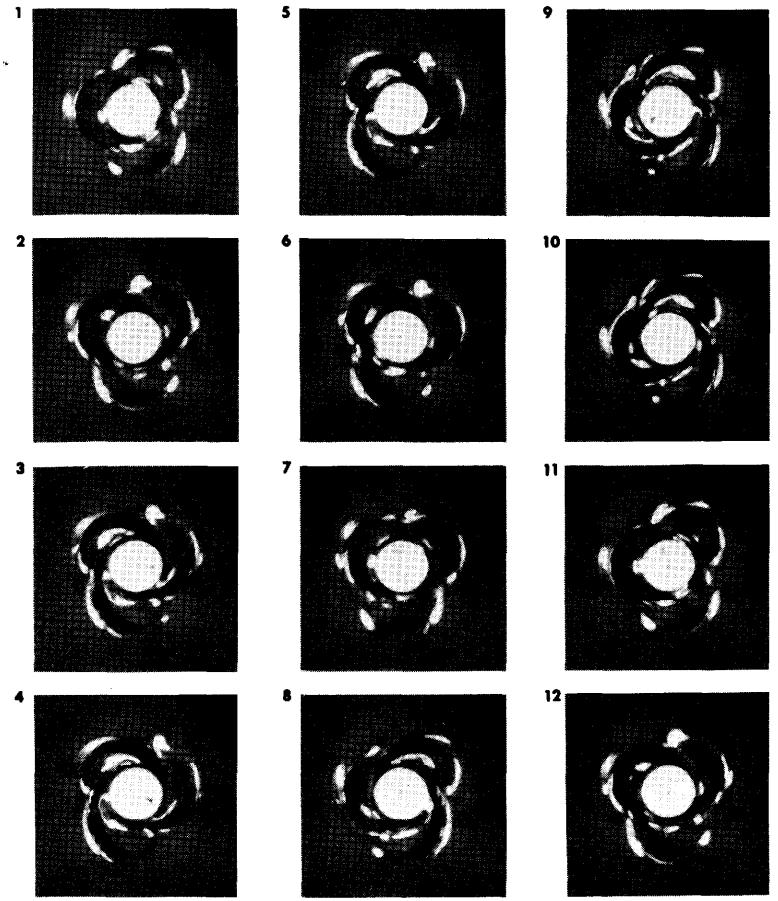

Fig. 9. Motion of the fully developed three-lobe flower instability of Fig. 8 as the rod goes through one complete cycle. Time between frames is approximately 0.015 sec. (Pictures taken from Ref. 6.)

height of climb at the rod increases monotonically with decreasing oscillation frequency, having a maximum value for steady rotation ($\Theta \to \infty, \omega \to 0$). This prediction of the analysis was found to be in very good agreement with our experiments. Here we examine the asymptotic form for the limit when the oscillation frequency becomes large at a fixed value of the amplitude $\varepsilon(\omega \to \infty, \Theta \to 0)$.

We begin with Eqs. (4) and (5) which define the complex function Λ, and observe that

$$\int_0^\infty G(s)e^{-i\omega s}ds = \frac{G(0)}{i\omega} - \frac{G'(0)}{\omega^2} - \int_0^\infty \frac{G''(s)e^{-i\omega s}}{\omega^2}ds.$$

Thus, for large ω, Eq. (5) gives

$$A^2 \sim \frac{i\rho\omega}{G(0)/i\omega - G'(0)/\omega^2}$$

or

$$A^2 \sim \frac{-\rho\omega^2}{G(0)}\left(1 + \frac{iG'(0)}{\omega G(0)}\right). \tag{11}$$

Then, from Eq. (4),

$$\lambda^2 \sim 1 - \frac{\rho a^2\omega^2}{G(0)}\left(1 + \frac{iG'(0)}{\omega G(0)}\right)$$

which for large ω can be written

$$\Lambda^2 \sim \frac{-\rho a^2}{G(0)}\left[\omega^4 + \left(\frac{G'(0)}{G(0)}\right)^2\omega^2\right]^{1/2}\exp(i\phi)$$

where $\tan\phi = G'(0)/\omega G(0)$. For large ω, $\phi \sim G'(0)/\omega G(0)$ and the equation for Λ has the form:

$$\Lambda \sim \left(\frac{\rho a^2}{G(0)}\right)^{1/2}\omega\exp\left[i\left(\frac{\pi}{2} + N\pi + \frac{G'(0)}{2\omega G(0)}\right)\right], \qquad N = 0,1.$$

We now write this in the form:

$$\lambda \sim \left(\frac{\rho a^2}{G(0)}\right)^{1/2}\omega\exp(iN\pi)\left(i\cos\frac{G'(0)}{2\omega G(0)} - \sin\frac{G'(0)}{2\omega G(0)}\right)$$

and observe from Eq. (7.6) of Part I that we require $\Lambda_r > 0$ and also $G'(0) < 0$, which requires that we take the branch with $N = 0$. So, for large values of ω,

$$\Lambda \sim \left(\frac{\rho a^2}{G(0)}\right)^{1/2}\left(i\omega - \frac{G'(0)}{2G(0)}\right), \tag{12}$$

and

$$\Lambda_r \sim -\frac{G'(0)}{2G(0)}\left(\frac{\rho a^2}{G(0)}\right)^{1/2}. \tag{13}$$

The equation for the mean climb $\bar{\bar{h}}(a)$ contains the parameter $\hat{\beta}_\Lambda$, and we thus require the form of the right-hand side of Eq. (3) for large ω. Integration by parts gives the following results for large ω:

$$\int_0^\infty G(s)\frac{\sin \omega s}{\omega}\,ds \sim \frac{G(0)}{\omega^2} \tag{14}$$

and

$$\int_0^\infty \int_0^\infty \gamma(s_1,s_2)\cos \omega(s_1 - s_2)ds_1\,ds_2 \sim \frac{\gamma(0,0)}{\omega^2}. \tag{15}$$

Thus, Eq. (3) becomes

$$\hat{\beta}_\Lambda \sim -(2\Lambda_r + 1)\,[G(0)/\omega^2] + (\Lambda_r + 1)[\gamma(0,0)/\omega^2]. \tag{16}$$

Substitution of Eqs. (11), (13), and (16) into Eq. (2) gives the asymptotic form for the normalized mean climb at the rod for $\omega \to \infty$:

$$H(a,\omega) = \frac{\bar{\bar{h}}}{\Theta^2} = \frac{\omega^2}{8}\frac{\lambda}{\rho g} \times \left(\frac{R^2[2G(0)(\Gamma R - 1) + \gamma(0,0)(2 - \Gamma R)]}{(2 - \Gamma R)(2 - \Gamma R + \lambda)} - \frac{RG(0)}{\Gamma(\Gamma R - \lambda)}\right) \tag{17}$$

where

$$\Gamma = G'(0)/G(0), \quad R^2 = \rho a^2/G(0), \quad \text{and} \quad \lambda^2 = \rho g a^2/T.$$

We cannot run our present apparatus at values of ω large enough to give an experimental test of Eq. (17). Moreover, our approximations of the material functions, if good, are good only in the integral sense explained below and are probably bad approximations of the values of $G(0)$ and $\gamma(0,0)$ needed in Eq. (17). Suppose, for example, that

$$G(s) = \sum_{n=1}^{N} \mu_n e^{-\alpha_n s}, \quad 0 < \alpha_1 < \alpha_2 < \cdots < \alpha_N. \tag{18}$$

Then

$$G(0) = \sum_{n=1}^{N} \mu_n, \tag{19}$$

but

$$\int_0^\infty G(s)\,ds = \sum_{n=1}^{N} \frac{\mu_n}{\alpha_n}. \tag{20}$$

It follows that the values of all μ_n's count with full force in Eq. (19) but are diminished by the factor $1/\alpha_n$ in Eq. (20).

This work was supported by the U.S. Army Research Office.

References

1. D. D. Joseph and G. S. Beavers, *Arch. Ration. Mech. Anal.*, **62**(4), 323 (1976) (Part I: Theory; Part II: Experiments).
2. L. D. Sturges and D. D. Joseph, *Arch. Ration. Mech. Anal.*, **64**(3), 245 (1977) (Part III: Oscillating planes).
3. D. D. Joseph and G. S. Beavers, *Rheol. Acta*, **16**(2), 169 (1977).
4. G. S. Beavers and D. D. Joseph, *J. Fluid Mech.*, **69**(3), 475 (1975).
5. G. S. Beavers and D. D. Joseph, *J. Fluid Mech.*, **81**(2), 265 (1977).
6. G. S. Beavers and D. D. Joseph, *Novel Weissenberg Effects*, 16-mm motion picture.

Received March 5, 1979
Accepted as revised January 17, 1980